SwimHR: Wearable-Free Heart Rate Monitoring for Swimmers via Water-Mediated ECG Sensing

Jiting Liu[1], Yue Gong[1], Zeyu Luo[1], Billy Chun Lung So[2], Qijia Shao[1*]
[1]The Hong Kong University of Science and Technology, Hong Kong SAR, China
[2]The Hong Kong Polytechnic University, Hong Kong SAR, China
{jliuie, ygongat, zluoay}@connect.ust.hk, billy.so@polyu.edu.hk, qijiashao@ust.hk

Abstract

Heart rate (HR) monitoring during swimming is crucial for athlete performance optimization and physiological assessment. Yet existing solutions remain unsatisfactory. ECG chest straps require tight skin contact and are often uncomfortable during swimming, while photoplethysmography (PPG) sensors suffer severe accuracy degradation due to swimming-induced motion artifacts. We present SwimHR, the first *wearable-free* HR monitoring system that captures electrocardiogram (ECG) signals transmitted through pool water without any on-body device. To enable practical pool-scale underwater ECG sensing, we (1) derive and validate a physical model of ECG transmission in water and quantify environmental attenuation in swimming pools through simulation, (2) design a lane-scale sensing architecture with a bias-electrode-free acquisition circuit for reliable full-lane coverage, and (3) develop a U-Net-based pipeline for robust R-peak detection under stroke-dependent swimming artifacts. We evaluate SwimHR with 34 swimmers (12 amateur and 22 professional) across four strokes and multiple pools. SwimHR achieves a mean HR error of 1.0 bpm with a standard deviation of 0.9 bpm relative to the ECG ground truth, significantly outperforming PPG-based wearables. SwimHR demonstrates the feasibility of accurate, real-time, wearable-free HR monitoring in standard swimming pool settings while avoiding the discomfort of body-worn sensors.

CCS Concepts

• **Hardware → Sensor devices and platforms**; • **Human-centered computing → Ubiquitous and mobile computing systems and tools**; • **Applied computing → Health care information systems**.

*Corresponding author.

This work is licensed under a Creative Commons Attribution 4.0 International License.
MobiCom '26, Austin, TX, USA
© 2026 Copyright held by the owner/author(s).
ACM ISBN 979-8-4007-2505-0/2026/10
https://doi.org/10.1145/3795866.3844450

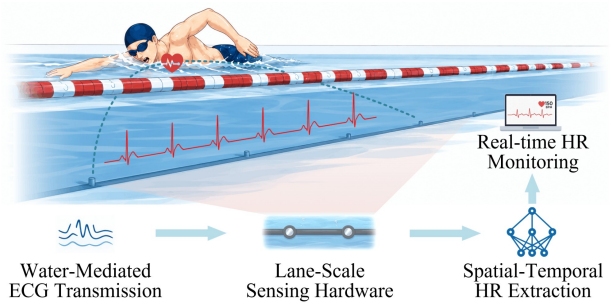

Figure 1: SwimHR enables wearable-free HR monitoring for swimmers by capturing ECG signals transmitted through pool water using proposed lane-scale electrodes and a spatial–temporal HR extraction pipeline.

Keywords

Underwater Sensing, Heart Rate, Electrocardiogram, Swimming, Wearable-Free Sensing

ACM Reference Format:
Jiting Liu[1], Yue Gong[1], Zeyu Luo[1], Billy Chun Lung So[2], Qijia Shao[1]. 2026. SwimHR: Wearable-Free Heart Rate Monitoring for Swimmers via Water-Mediated ECG Sensing. In *The 32nd Annual International Conference on Mobile Computing and Networking (MobiCom '26), October 26–30, 2026, Austin, TX, USA.* ACM, New York, NY, USA, 16 pages. https://doi.org/10.1145/3795866.3844450

1 Introduction

Heart rate (HR) is one of the most important physiological signals for monitoring human health and physical exertion in aquatic environments. In swim training, coaches use HR to quantify training load, recovery, and interval intensity, while swimmers use it to optimize training intensity and avoid overtraining [46, 49]. Yet obtaining accurate HR during swimming remains surprisingly inconvenient. Existing practice is dominated by wearable devices, but both major options are problematic underwater. ECG chest straps must be worn tightly to maintain contact during turns and high-intensity sets, which is often uncomfortable and distracting [11]. PPG-based sensors worn on the wrist, forearm, temple are more convenient, but are highly sensitive to motion, water disturbance, and changes in the optical path underwater [7, 40]. Moreover, current wearables mostly expose HR only after

the session because they cannot transmit data wirelessly underwater, limiting their value for real-time coaching.

Since water is conductive, an intriguing possibility is to use pool water itself as the sensing medium for ECG, eliminating the need for swimmers to wear any device. Prior studies have shown that ECG can propagate through water, but only in very confined settings [19, 25, 26, 63] such as bathtubs, with stationary users and electrodes placed close to the body (e.g., 5 cm). These feasibility demonstrations do not address the conditions that matter in real swimming: meter-scale swimmer-to-electrode distance, full-lane coverage, strong stroke-dependent motion, and standard-pool environments with varying conductivity and grounded metallic structures. As a result, it remains unclear whether water-mediated ECG can support accurate, real-time, wearable-free HR monitoring for swimmers in standard pools.

In this paper, we present *SwimHR*, to the best of our knowledge, the first wearable-free system that continuously monitors swimmers' HR in real time via water-mediated ECG sensing in standard swimming pools. As shown in Figure 1, SwimHR captures ECG signals transmitted through pool water using lane-scale underwater rope electrodes, without any device on the swimmer's body. At a high level, SwimHR combines physical modeling of pool-scale ECG transmission, deployable sensing hardware, and spatial-temporal signal inference to recover R-peaks and HR during active swimming.

Designing such a system requires overcoming three key challenges. First, pool-scale water-mediated ECG is extremely weak and strongly environment-dependent. Second, a practical system must provide stable full-lane coverage and low-noise acquisition without any on-body bias electrode, even though conventional ECG front-ends assume a third electrode attached to the body. Third, active swimming produces severe non-stationary artifacts from body motion, turbulence, and changing swimmer-electrode coupling as the swimmer moves through the lane; these artifacts vary across strokes, making fixed-threshold peak detection unreliable.

SwimHR addresses these challenges with three corresponding designs. First, we derive and validate a quasi-static dipole model of ECG transmission in water and use simulation to quantify environmental attenuation in standard pools. These results explain why pool-scale signals are much weaker than bathtub signals and directly guide our sensing geometry and hardware design. Second, we design a lane-scale sensing hardware with same-side underwater rope electrodes and a bias-electrode-free acquisition circuit that preserves always-available ECG sensing along the lane and a fully wearable-free setup. Third, we design a spatial–temporal HR extraction pipeline that dynamically selects informative channels, uses a U-Net-based model to locate R-peaks under amplitude variation and motion artifacts, and applies temporal consistency filtering for stable HR estimation.

We implement SwimHR prototypes and evaluate them with 34 swimmers (12 amateur and 22 professional) across two public swimming pools and four competitive strokes, covering more than 32,000 m of swimming. Across all recordings, SwimHR achieves a mean HR error of 1.0 bpm and standard deviation of 0.9 bpm relative to a Polar H10 ECG reference. In contrast, commonly used PPG-based wearables (i.e., Apple Watch and Polar Verity Sense) exhibit substantially higher errors (e.g., 5.4 bpm) and larger performance variability (e.g., standard deviation 7.7 bpm), with further degradation during high-motion strokes such as butterfly. SwimHR maintains high accuracy across strokes (0.8 bpm for breaststroke, 0.9 bpm for freestyle, 0.8 bpm for backstroke, and 1.6 bpm for butterfly) and generalizes across swimmer groups and pool environments. Participants also report significantly higher comfort than with wearable baselines. A demonstration video of SwimHR is available at:

https://youtu.be/pYqvvz1_QZ0

We summarize our contributions as follows:

- To the best of our knowledge, SwimHR is the first system capable of continuously estimating swimmers' HR in standard swimming pools without any on-body device.
- We derive and experimentally validate a quasi-static dipole water-mediated ECG transmission model, and use simulation to quantify environmental attenuation factors.
- We design underwater sensing hardware with same-side rope electrodes and a bias-free acquisition circuit, enabling stable ECG capture across the swimming lane.
- We propose a channel-aware HR detection pipeline that combines adaptive channel selection, U-Net–based R-peak detection, and temporal consistency filtering to robustly extract heart rate under stroke-dependent motion artifacts.
- We build SwimHR prototypes and evaluate them with 34 swimmers across four competitive strokes and two public swimming pools. SwimHR achieves accurate and robust HR monitoring, significantly outperforming commercial wearable baselines, and is strongly preferred by participants for its wearable-free design.

More broadly, SwimHR demonstrates that aquatic infrastructure can serve as a practical substrate for wearable-free physiological sensing, opening new opportunities for training analytics and unobtrusive health monitoring in water.

2 Background and Challenges

2.1 ECG Primer

Electrocardiography (ECG) measures the electrical activity generated by the depolarization and repolarization of cardiac muscle cells [16, 33, 53]. These electrical currents propagate through surrounding conductive tissues and create measurable biopotentials on the body surface [10, 51, 52]. The ECG waveform exhibits characteristic components (P-wave, QRS

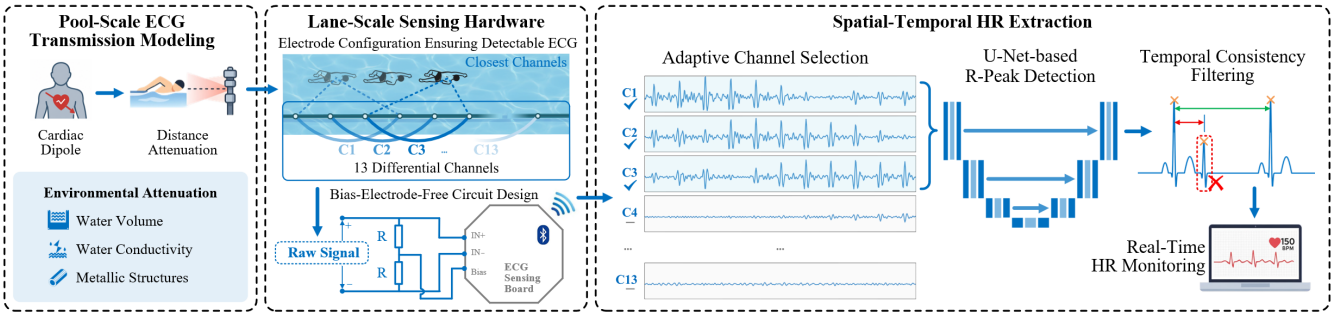

Figure 2: SwimHR System Overview.

complex, and T-wave) corresponding to phases of the cardiac cycle. Among them, the R-peak in the QRS complex is the most prominent feature and is widely used for heart-rate (HR) estimation by measuring the interval between consecutive R-peaks [31]. Traditional ECG acquisition places electrodes on the skin to measure the potential difference between two points on the body, often using a third bias or driven-right-leg (DRL) electrode to stabilize the common-mode voltage and suppress ambient interference in biopotential acquisition systems [3]. When the human body is immersed in water, the cardiac electrical field can propagate beyond the body surface into the surrounding conductive medium [19, 25, 26, 63]. As a result, electrodes placed in water can capture ECG signals without direct skin contact. This property enables wearable-free ECG sensing underwater and forms the physical basis for the system design in this work.

2.2 Challenges

Extending water-mediated ECG sensing from confined settings to real swimming scenarios with different strokes in standard pools poses several fundamental challenges.

Signal Attenuation and Environmental Dependence. Compared to bathtub-scale demonstrations, a swimming pool introduces meter-scale swimmer-to-electrode distances and a substantially larger conductive volume, which together significantly reduce the measurable differential biopotential. Moreover, the received signal strength depends on pool-specific environmental conditions, such as water conductivity and electrically grounded metallic structures, making the channel highly different from controlled small-volume settings. Without understanding this pool-scale transmission behavior, it is unclear what signal strength to expect and how to design a reliable sensing system.

Difficult Lane-Scale Deployment. A feasibility setup can acquire underwater ECG using a small number of electrodes. However, monitoring a swimmer during laps requires *full-lane coverage*, and deploying multiple independent electrode units throughout the pool to guarantee coverage is logistically intensive and disruptive to normal pool operation. In addition, pool-scale underwater ECG exhibits low signal-to-noise ratio (SNR), demanding high-gain, low-noise acquisition. Finally, standard ECG front-ends typically rely on a third bias (driven-right-leg) electrode in skin contact to stabilize the input common-mode voltage and prevent ADC saturation. A wearable-free system must therefore provide a deployable lane-scale sensing configuration and achieve stable, low-noise acquisition *without any on-body bias electrode*.

Non-stationary Swimming Artifacts. Active swimming introduces strong, time-varying artifacts from body motion, breathing, turbulence, and changing coupling as the swimmer moves along the lane. Different strokes and intensities induce qualitatively different artifact patterns, which can obscure QRS complexes and cause false peaks or missed beats. The system must therefore reliably extract R-peaks and heart rate across strokes under highly non-stationary noise.

3 System Design

To address the challenges in Section 2, SwimHR consists of three key components. First, we model ECG transmission in water at the pool scale and quantify the effects of environmental factors on signal attenuation, providing the foundation for subsequent hardware and algorithm design. Second, we design a deployable lane-scale sensing architecture with a bias-electrode-free, low-noise acquisition circuit to enable stable wearable-free ECG capture during swimming. Third, we develop a U-Net-based inference pipeline to robustly detect R-peaks under swimming artifacts and estimate heart rate across strokes. Figure 2 illustrates the system overview, and we describe these components next.

3.1 Pool-Scale ECG Transmission Modeling

Water-mediated ECG sensing in a standard swimming pool is fundamentally different from prior bathtub-scale feasibility demonstrations. To guide the design of SwimHR, we first develop a physical model of ECG transmission in water, then validate it experimentally, and finally use simulation to quantify how pool environments affect signal strength.

Quasi-static Transmission Model. To model ECG transmission in water, we first examine how cardiac electric fields

propagate through the conductive pool environment. Two types of currents may arise in an electric field: conduction current and displacement current [13, 15]. The conduction current density follows Ohm's law: $J_c = \sigma E$, where J_c is the conduction current density, σ is the water conductivity, and E is the electric field strength. In contrast, displacement current results from time-varying electric fields and is given by $J_d = \epsilon \frac{\partial E}{\partial t}$, where ϵ denotes the permittivity. Whether displacement current must be considered depends on the ratio between displacement and conduction currents [12, 54, 65]:

$$\frac{|J_d|}{|J_c|} = \frac{\epsilon}{\sigma}\omega = \frac{\epsilon_r \epsilon_0}{\sigma}\omega, \tag{1}$$

where $\omega = 2\pi f$ is the angular frequency.

In swimming pools, water conductivity typically ranges from 0.02 to 0.1 S/m [35, 48], the relative permittivity of water ϵ_r is 78.3 [30], the vacuum permittivity ϵ_0 is $8.85\times10^{-12}\ F\cdot m^{-1}$, while ECGs occupy a low-frequency band of approximately 0.05–100 Hz [57]. Under these conditions, $\frac{\epsilon}{\sigma} \approx 10^{-8}$, making $\frac{|J_d|}{|J_c|} \ll 1$. Therefore, displacement currents are negligible, and ECG transmission in pool water can be modeled as a *quasi-static conduction process*. This result allows us to model the water as a conductive volume and analyze ECG propagation using a dipole-based electric potential model, as described next.

Dipole-based ECG Transmission in Water. Given the validated quasi-static assumption above, we model the swimmer and surrounding water as a conductive volume and represent the heart as an equivalent current dipole [33]. Under this model, the electric potential at any point in water is determined by the relative geometry between the sensing location and the dipole source.

For a monopole current source with strength I_0, the conduction current density at a distance r is $J_c = I_0/(4\pi \cdot r^2)$ [32]. Combining this with Ohm's law yields the electric field strength: $E = I_0/(4\pi\sigma \cdot r^2)$. The potential generated by the monopole current source can be expressed as:

$$V = -\frac{I_0}{4\pi\sigma} \cdot \int_{\infty}^{r} \frac{1}{r^2} dr = \frac{I_0}{4\pi\sigma} \cdot \frac{1}{r} \tag{2}$$

We then model the heart as a dipole with a positive and a negative pole. The potential at an arbitrary point i is the superposition of the two poles:

$$V_i = V_+ + V_- = \frac{1}{4\pi\sigma} \cdot \left(\frac{I_0}{r_{i+}} + \frac{-I_0}{r_{i-}}\right) \tag{3}$$

where r_{i+} and r_{i-} are the distances from the positive and negative poles, respectively. Since ECG signals are computed as the differences in biopotentials between two electrodes, i and j, the underwater ECG signals can be defined by

$$V_{ECG} = V_i - V_j = \frac{I_0}{4\pi\sigma} \cdot \left(\frac{1}{r_{i+}} - \frac{1}{r_{i-}} - \frac{1}{r_{j+}} + \frac{1}{r_{j-}}\right) \tag{4}$$

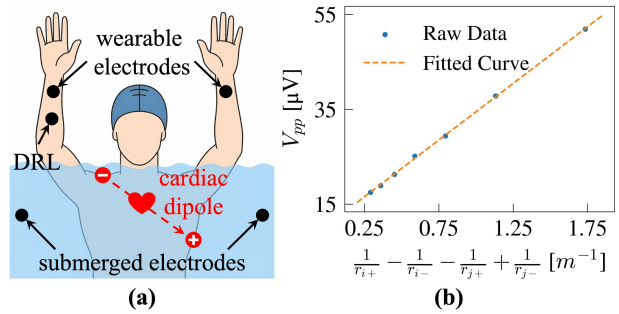

Figure 3: (a) The experiment setup and cardiac dipole geometry for the transmission model validation. (b) V_{pp} is linearly related to $(\frac{1}{r_{i+}} - \frac{1}{r_{i-}} - \frac{1}{r_{j+}} + \frac{1}{r_{j-}})$ in Eq. (4).

In the underwater scenario, I_0 denotes the effective cardiac current coupled into water. As illustrated in Figure 3(a), the positive and negative poles of the dipole are defined by the intersections between the body surface and the heart orientation. We assume that the heart lies near the body midline [59] and approximate the dipole axis using the principal anatomical heart axis [36]. Equation (4) shows that the received ECG strength depends jointly on water conductivity and swimmer-electrode geometry, motivating both our lane-scale sensing design and the environmental attenuation analysis.

Experiment Validation. We validate the transmission model in Eq. (4) through a controlled study in a semi-Olympic swimming pool with a depth of 1.5 m and a water conductivity of 0.045 S/m, measured using a portable conductivity meter (KEDIDA CT-3030) [23]. As shown in Figure 3(a), two underwater electrodes are placed symmetrically around the swimmer, and the distance between two electrodes is varied from 1.0 m to 2.5 m in 0.25 m increments, with the heart approximately located at the midpoint. A reference ground truth ECG channel with a driven-right-leg (DRL) electrode is recorded simultaneously outside the water.

We quantify signal strength using the ECG peak-to-peak amplitude V_{pp}. According to Eq. (4), the ECG amplitudes vary linearly with the geometric term $x = \left(\frac{1}{r_{i+}} - \frac{1}{r_{i-}} - \frac{1}{r_{j+}} + \frac{1}{r_{j-}}\right)$ We therefore fit the measured V_{pp} using the model $y = k(x + e)$, where k captures subject-dependent and environment-dependent factors.

As shown in Figure 3(b), the experimental results confirm an approximately linear relationship between V_{pp} and the geometric term predicted by the model. The fitted parameters are $k = 23.87$ and $e = 0.44$, which correspond to an effective cardiac source strength of 0.57 μA considering an acquisition gain of 24. This effective value is subject- and environment-dependent and does not represent the intrinsic cardiac source current. This validation demonstrates that the proposed model captures the first-order transmission

behavior of underwater ECG signals in swimming pools and provides a practical basis for our rope electrode design.

Environmental Attenuation Analysis. While the transmission model captures how geometry and conductivity affect signal strength, it does not fully explain the large gap between bathtub and pool measurements. In a bathtub experiment with the same subject and a 0.5 m electrode spacing, the ECG amplitude reaches 688.1 μV but drops to 98.3 μV in the pool, indicating additional environmental attenuation.

To investigate this effect, we simulate pool-scale ECG transmission using a 3-D cardiac electrical activity model [55] implemented in COMSOL [34]. The model places a cardiac dipole inside a 5 m×5 m×1.5 m conductive pool with symmetrically positioned electrodes, and varies key environmental parameters to quantify their influence on the received signal. More details are provided in the Appendix, and the simulation code will be released to support future research.

The simulation identifies three main attenuation factors. Larger *water volume* spreads the electric field over a larger conductive region, reducing the measurable potential difference. Higher *water conductivity* further attenuates the signal, as σ appears in the denominator of Equation 4. Finally, *metallic structures* (e.g., ladders), which are grounded for safety in pools [8, 17, 37, 38, 66], can distort the electric field and significantly reduce signal strength when in direct contact with water.

Overall, these environmental factors attenuate the ECG signal by approximately 7.2× in simulation, consistent with the around 7× attenuation observed in our pool measurements. This result highlights that pool-scale ECG sensing operates under much weaker signals than confined environments, motivating the high-gain sensing hardware and robust signal inference pipeline described next.

3.2 Lane-Scale Sensing Hardware

To address the deployment and low-SNR challenges, SwimHR introduces a lane-scale sensing hardware design that enables stable underwater ECG acquisition without requiring any on-body electrodes. The hardware design consists of two components: always-available underwater rope electrodes and a bias-electrode-free acquisition circuit.

Always Available Same-Side Rope Electrodes. The transmission model shows that ECG signal strength decreases rapidly as the swimmer-electrode distance increases. A practical sensing system must therefore ensure that, wherever the swimmer is along the lane, nearby electrodes remain available and the sensing distance stays short and stable.

To achieve this, we propose a *same-side* lane-scale electrode design as shown in Figure 2. Instead of placing electrodes on opposite sides of the swimmer as in traditional ECG systems, we pair electrodes along a single lane rope on the same side of the swimmer. This design is enabled by the transmission model derived in Section 3.1, which shows that electrodes closer to the swimmer experience a higher electric potential than those farther away, allowing ECG sensing through the spatial potential gradient along the swimming lane. Compared with a bilateral design, the same-side configuration provides two additional advantages. First, it reduces motion-induced noise: water flow and rope vibration can introduce electrochemical disturbances and electromagnetic interference [5, 9, 61], but electrodes on the same rope experience more correlated motion, allowing partial cancellation in the differential ECG signal. Second, it simplifies deployment by requiring only a single sensing structure rather than two synchronized installations on both sides of the lane.

We also integrate this design directly into modified lane ropes as the sensing electrodes. A lane rope consists of a stainless-steel cable encased in a plastic sheath. We expose a short segment of the stainless-steel cable so that it directly contacts the surrounding water and acts as a sensing electrode, while the remaining insulated portion preserves electrical isolation along the transmission path. Stainless steel provides reliable signal quality for dry electrode sensing and is suitable for long-term aquatic deployment [21, 22]. These submerged electrodes are passive and inject no current into the water; all powered electronics remain on the pool deck.

As shown in Figure 4, we place electrodes at 1 m intervals along the lane, ensuring that the swimmer is always near multiple sensing electrodes during swimming. Although increasing the sensing distance between a pair of electrodes can increase the measured differential potential, it also reduces the correlation between their motion-induced artifacts, weakening noise cancellation in the differential measurement. Our measurements show that a 3 m separation provides the best trade-off between signal strength and motion robustness, yielding the highest SNR. We therefore form each differential channel using two electrodes separated by 3 m. In a standard 25 m pool, 25 electrodes are deployed, indexed from $E1$ to $E25$, and divided into four groups to avoid forming redundant overlapping channels across adjacent groups. Within each group, the electrodes are paired with the corresponding electrodes 3 m away, producing three differential channels (e.g., $E1 \leftrightarrow E4$, $E2 \leftrightarrow E5$, $E3 \leftrightarrow E6$). To cover the final meter of the lane, $E22$ is additionally paired with $E25$. This configuration forms 13 differential channels in total.

Bias-electrode-free Acquisition Circuit. Conventional ECG acquisition systems use a third electrode, commonly referred to as the driven-right-leg (DRL) electrode, to stabilize the input common-mode voltage and suppress ambient interference [14, 60]. The DRL circuit senses the common-mode component of the differential inputs and feeds back a

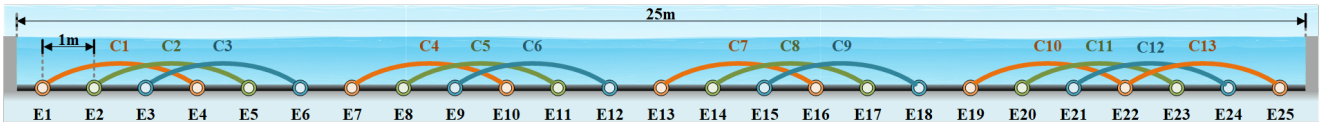

Figure 4: Full-lane coverage using 25 electrodes (E1–E25) to form 13 differential sensing channels (C1–C13).

compensating signal to the body, reducing power-line interference and keeping the input voltage within the operating range of the analog-to-digital converter (ADC). For example, the ADS1299 biopotential acquisition chip [18] we employed requires the input common-mode voltage to satisfy $V_{dd} - 0.2V - \left(\frac{GV_{in}}{2}\right) > V_{cm} > V_{ss} + 0.2V + \left(\frac{GV_{in}}{2}\right)$. Here V_{dd} and V_{ss} represent the positive and negative power supplies, respectively; V_{cm} is the common-mode voltage; G is the gain of the amplifier; V_{in} is the maximum differential input signal; and $0.2V$ accounts for the amplifier headroom. In our scenario, attaching a bias electrode to the swimmer would violate the wearable-free design goal. We therefore design a bias-electrode-free acquisition circuit that stabilizes the input common-mode voltage without direct body contact. Inspired by prior two-electrode ECG designs [3], we redirect the DRL feedback path to the differential input nodes through high-value (10 MΩ) resistors. These resistors provide a weak bias path that stabilizes the input common-mode voltage without requiring direct body-electrode contact. Only the passive rope electrodes and their connecting cables are submerged, while the custom bias-electrode-free PCB and signal acquisition board remain on the pool deck. This arrangement enables stable water-mediated ECG acquisition without any on-body device, while supporting continuous data transmission for real-time HR monitoring. Together, the deployable rope electrodes and bias-electrode-free front end form the hardware foundation of SwimHR.

3.3 Spatial–Temporal HR Extraction

Active swimming introduces strong motion artifacts and spatially varying signal quality. As swimmers move along the lane, the ECG signal strength shifts across sensing channels because the electrodes are spaced 1 m apart as we discussed in Section 3.2. At any given moment, only a small subset of nearby electrodes captures usable signals. Reliable HR estimation therefore requires dynamically selecting informative channels while suppressing motion-induced noise. We design a spatial–temporal HR extraction pipeline including three stages: (1) adaptive channel selection, (2) U-Net-based R-peak detection, and (3) HR estimation with temporal filtering. Algorithm 1 summarizes the overall procedure.

Adaptive Channel Selection. Due to the 1 m electrode spacing, ECG signals are typically observable in three adjacent channels at a time, while signals in distant channels are too weak to detect. Instead of processing all channels, we dynamically identify the most informative ones. We first apply a bandpass filter (10–30 Hz) to remove motion artifacts and baseline drift, while also reducing EMG interference. Then, for each 4-second signal window (with a 1-second stride), we detect candidate R-peaks using NeuroKit2 [29]. Each channel and its inverted signal are processed to account for waveform polarity changes during bidirectional swimming. A candidate is retained only if its amplitude exceeds 1 μV and its local signal-to-noise ratio exceeds 6 dB, where

Algorithm 1 Spatial–Temporal HR Extraction

Require: Multi-channel ECG signals $\mathbf{X}$, window length $T_w = 4$s, step size $T_s = 1$s
Ensure: Heart-rate estimates $\mathbf{H}$

```
H ← ∅
for each window w of X with length T_w and step T_s do
    Stage 1: Adaptive Channel Selection
    for each channel c in w do
        Detect peaks in w_c and −w_c using ecg_peaks
        Keep peaks with amplitude ≥ 1 μV and SNR ≥ 6 dB
    end for
    Cluster cross-channel candidates within 64 ms
    Score each adjacent three-channel set by its summed cluster count
    Select the best set C* adjacent to C_prev
    C_prev ← C*
    Stage 2: U-Net based R-Peak Detection
    Z-score normalize the selected channels
    Apply U-Net to w(C*) to obtain probability mask ŷ
    Keep ŷ > 0.5 regions with ≥ 10 samples
    Select the sample with max absolute amplitude per region as the R-peak R
    Stage 3: Temporal Consistency Filtering
    Compute RR intervals ΔR from R
    If < 0.5ΔR_exp, keep the better-fitting peak
    Split at RR > 1.5ΔR_exp while retaining RR history
    for each valid peak segment s do
        Compute HR h_s with 3 consecutive RR intervals
        Accept h_s that 60 < h_s < 200 and |Δh_s| ≤ 5
        H ← H ∪ {h_s}
    end for
end for
return H
```

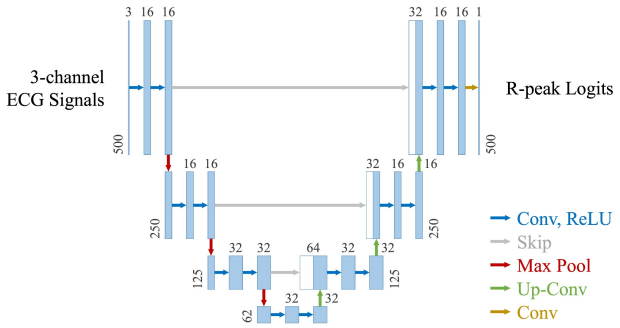

Figure 5: U-Net for segmentation-based R-peak detection. The numbers inside the blocks denote the temporal feature length at each resolution.

the ratio compares the standard deviation within the central 0.1 s peak region with that of the two adjacent 0.2 s regions.

We aggregate the surviving detections across channels and cluster detections occurring within 64 ms as the same heartbeat, allowing each channel to contribute at most one detection to each cluster. To preserve spatial coherence, every three adjacent channels form a candidate set, which is scored by summing the heartbeat-cluster counts across its three channels. For each 4-second window, we select the highest-scoring candidate set under a temporal continuity constraint: the selected set must remain adjacent to the set chosen in the previous window, reflecting the swimmer's continuous movement. The spatial grouping and temporal continuity constraint suppress noise-induced selections and ensure that the selected channels track the swimmer's location.

U-Net-based R-peak Detection. After selecting the informative channels, the next step is to accurately locate R-peaks under residual motion artifacts and time-varying signal amplitudes. The transmission model in Section 3.1 shows that underwater ECG amplitude varies with swimmer-electrode geometry as the swimmer moves along the lane. As a result, detectors based on fixed signal-amplitude thresholds are unreliable. To further reduce sensitivity to amplitude variation, each selected channel is independently z-score normalized.

To solve this problem, we design a U-Net architecture inspired by prior work [64] that learns the temporal morphology of ECG waveforms. As shown in Figure 5, the model takes a 4-second window from the three selected channels as input and outputs a one-dimensional binary mask indicating R-peak locations. The encoder progressively downsamples the input to aggregate context over multiple temporal scales, while the decoder restores temporal resolution for precise localization. Specifically, the encoder contains four resolution levels with temporal kernel sizes 7, 5, 3, and 3 and feature dimensions of 16, 16, 32, and 32, respectively. Each level contains two one-dimensional convolution layers, each followed by batch normalization, ReLU activation, and 2× max pooling. Starting from the 500-sample (i.e., 4-second) input window, the feature length is reduced from 500 to 250, 125, and 62 samples. The decoder mirrors this structure using transposed convolutions to restore the temporal resolution to 500 samples. Skip connections link encoder and decoder features at matching resolutions, preserving fine-grained waveform details that are critical for accurate R-peak localization. A final convolution layer produces one logit per sample, which is converted into an R-peak probability using a sigmoid function. The resulting lightweight network contains approximately 38,497 trainable parameters.

To train the model, we construct a labeled dataset of R-peaks from swimming recordings. Training labels are generated from manually annotated R-peaks collected in five 50 m breaststroke sessions per swimmer by an experienced annotator. Because R-peaks occupy only a small fraction of the signal, the dataset is highly imbalanced. To mitigate this issue, each annotated R-peak is expanded into a 0.16 s window during training, increasing the proportion of positive labels while accounting for small temporal misalignments. The model is optimized using binary cross-entropy with logits and the Adam optimizer with a learning rate of 10^{-3}.

We train the model by leave-one-user-out cross-validation. In each fold, one swimmer's data is reserved for testing, while the remaining swimmers' first four 50 m breaststroke sessions are used for training, and their fifth sessions are used for validation. Training runs for up to 100 epochs with a batch size of 64 and early stopping with a patience of 10 epochs without improvement in the validation per-sample F1 score. The model achieves a mean per-sample validation F1 score of 97.03%.

During inference, the sigmoid probability sequence is thresholded at 0.5 to form contiguous candidate regions. Regions shorter than ten samples are discarded as noise. Within each remaining region, the precise R-peak location is selected as the sample with the largest absolute amplitude across the three selected channels.

HR Estimation with Temporal Filtering. After R-peak locations are detected, HR is estimated from the RR intervals. The instantaneous HR is computed from the average of three consecutive RR intervals. To suppress spurious detections caused by motion artifacts, we maintain a sliding buffer of the five most recent RR intervals and compute the expected RR interval as the median of this buffer. When a new peak occurs within 0.5× the expected interval, the algorithm retains either the new peak or the preceding accepted peak, depending on which produces an interval closer to the expected rhythm. If the interval to the next detected peak exceeds 1.5× the expected RR interval, we treat it as a transient signal break rather than compensating for a missed detection. In this case, the peak sequence is split into separate

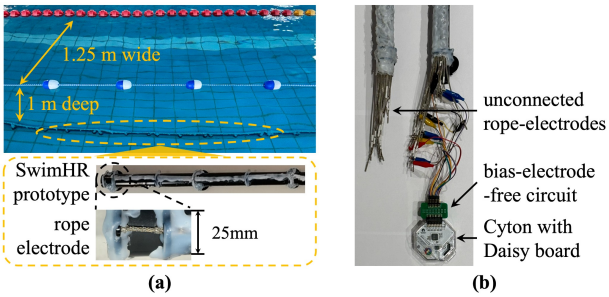

Figure 6: (a) SwimHR prototype is deployed at Pool A. (b) The rope electrodes are connected to the bias-electrode-free circuit and OpenBCI board.

segments, and HR is computed independently within each segment. The recent RR buffer is retained across the break to preserve the previous rhythm as an adaptive reference. The resulting estimates are Gaussian-smoothed. Overall, the temporal filtering reduces false detections and prevents error propagation during brief signal loss.

4 Prototype Implementation

We implement SwimHR prototypes using commercially available components, prioritizing sensing stability, corrosion resistance, compatibility with standard swimming pools.

Underwater sensing structure. As shown in Figure 6(a), the underwater sensing structure consists of PVC support pipes and plastic-coated steel cables that serve as electrodes. PVC was selected for its corrosion resistance, low weight, and mechanical robustness in aquatic environments. The sensing electrodes were positioned approximately 1 m below the water surface. Twenty-five electrodes are distributed along the 25 m lane at 1 m intervals (from 0.5 m to 24.5 m). Each electrode is created by stripping a 1 cm section of insulation from the plastic-coated steel cable to expose the conductive core to the surrounding water. The cables are attached to the PVC structure using hot-melt adhesive to ensure water resistance and mechanical stability. To further suppress motion-induced noise, the sensing rope is stabilized using rigid plastic supports anchored to the pool floor with suction cups, enabling a non-destructive installation compatible with existing swimming pools.

Signal acquisition unit. ECG signals are acquired using an OpenBCI Cyton board with a Daisy extension [41]. The system samples signals at 125 Hz and transmits data to a host computer via Bluetooth Low Energy. In total, 13 differential ECG channels are used for sensing. To implement the proposed bias-electrode-free circuit, we designed a compact custom printed circuit board (Figure 6(b)) that interfaces between the electrodes and the OpenBCI inputs. The PCB (37 mm × 20 mm) includes 16 signal paths, each incorporating a 10 MΩ resistor to implement the bias feedback network.

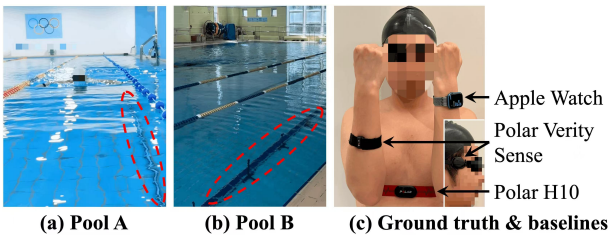

Figure 7: SwimHR deployed at Pool (a) A and (b) B. (c) Participant wears ground truth and baseline sensors.

The OpenBCI channels are connected to the steel electrodes through the PCB using clip-to-Dupont jumper wires, enabling reliable signal acquisition while maintaining electrical isolation from the swimmer. The prototype costs $600 USD in total, primarily for OpenBCI circuit boards ($450).

5 System Evaluation

We evaluate SwimHR in swimming pools to characterize its HR estimation accuracy, robustness across swimmer populations, swimming strokes, pools, and its practicality for real-world deployment. All human-subject experiments were approved by our institution's Institutional Review Board.

5.1 Study Setup

Deployment Environments. We deploy SwimHR in two public swimming pools (Figure 7) with different geometries and depth profiles. Pool A measures 25 m × 12.5 m, with depth varying from 1.0 m to 1.6 m. Its water conductivity and temperature are 0.078 S/m and 25°C, respectively. Pool B measures 25 m × 15 m, with a non-uniform depth profile: 1.2 m at one end, increasing to 1.5 m at the center, and returning to 1.2 m at the opposite end. Its water conductivity and temperature are 0.068 S/m and 25°C, respectively. The sensing prototype is placed at the center of a standard 2.5m-wide swimming lane, with a temporary lane divider installed directly above it to define the instrumented swimming region.

Participants. We recruit 34 swimmers with two skill levels: 12 skilled amateur swimmers and 22 professional swimmers. The professional swimmers include certified lifeguards, swimming coaches, and elite competitive swimmers who have participated in national-level competitions. Thirty-two swimmers (10 amateurs and 22 professionals) participate in Pool A, and five amateurs participate in Pool B; three amateurs participate in both pools to support cross-pool validation. All professional swimmers are proficient in all four competitive strokes (i.e. breaststroke, freestyle, backstroke, and butterfly). To ensure safety, all participants are healthy and report no medical conditions or physical discomfort, and a certified lifeguard monitors all sessions. Participants wore

Table 1: Participants and Data.

	Amateur	Professional
Gender	8 males, 4 females	18 males, 4 females
Age, 18–24	6	1
25–34	5	11
35–44	1	8
45–54	0	2
Certificate	amateur level	20 coaches/lifeguards 2 elite swimmers
Strokes	breaststroke only	All four strokes
Total Data	7,450 meters 228.7 minutes	25,425 meters 565.4 minutes

their own swimsuits throughout the study, and no swimsuit-related degradation in signal capture was observed. We summarize the detailed participant characteristics in Table 1.

Experimental protocol. The protocol is designed to balance data diversity with swimmer safety. The amateur swimmers perform breaststroke only, which is their preferred stroke, and each completes 500 m, divided into ten 50 m segments with rest intervals. Professional swimmers perform all four competitive strokes to evaluate system performance under different body motions. For breaststroke, freestyle, and backstroke, swimmers complete continuous 50 m segments. Butterfly is substantially more demanding, so participants may perform either continuous 50 m segments or split each 50 m trial into two 25 m segments with a rest in between. All professional swimmers complete at least 100 m of butterfly.

A typical study session lasts approximately 30 minutes for amateur swimmers and 60 minutes for professional swimmers, including rest periods between segments. After excluding recordings affected by ground-truth device failures, the final evaluation dataset (summarized in Table 1) comprises 7,450 m (228.7 minutes) of breaststroke data from amateur swimmers and 25,425 m (565.4 minutes) from professional swimmers, including 10,650 m (241.6 minutes) of breaststroke, 5,350 m (105.2 minutes) of freestyle, 5,350 m (136.8 minutes) of backstroke, and 4,075 m (81.8 minutes) of butterfly. During each trial, only one participant swims in the instrumented lane, while the adjacent lanes remain open for normal pool use.

Ground Truth and Wearable Baselines. All participants wear a Polar H10 ECG chest belt [43] as the ground-truth reference. To benchmark SwimHR against PPG-based commercial wearables, we select three baselines with different form factors and body locations: (1) an Apple Watch Series 7 [1] on the left wrist, (2) a Polar Verity Sense [44] on the right forearm, and (3) a second Polar Verity Sense mounted at the right temple using the goggle-strap clip. As shown in Fig. 7(c), participants wear all four devices simultaneously in the study. This setup covers both mainstream consumer wearables and swimming-oriented optical sensors. The Polar H10 measures ECG through chest electrodes and is widely regarded as a gold-standard wearable for heart-rate monitoring during swimming [4, 7]. The Apple Watch represents the dominant smartwatch form factor. The Polar Verity Sense is a compact waterproof optical sensor that supports flexible placement; we evaluate both forearm and temple locations because the temple typically experiences less motion than the limbs and is already used by some professional swimmers in practice. Since none of these wearable devices can transmit data wirelessly underwater, they all store HR data locally. Before each trial, we adjust device placement and tightness with each participant to ensure comfort and stable contact, and inspect all sensors after each 50 m segment.

Evaluation Metrics. We evaluate heart rate estimation using two metrics. First, we report the mean absolute error (MAE) with respect to the ground-truth reference, since heart rate is computed on a per-second basis. Second, we report the standard deviation (std) of MAE across recordings to quantify temporal stability and performance consistency. Baseline performance is computed using the same metrics by comparing each baseline against the ground-truth reference.

5.2 HR Estimation Performance

We evaluate the HR estimation accuracy of SwimHR and all wearable baselines against the Polar H10 reference. All devices provide HR time series on a nominal 1-Hz timeline. The Apple Watch intermittently omits samples, so we forward-fill each missing entry using its most recently reported HR value. Because commercial devices do not disclose their internal estimation windows or output latency, we account for a possible constant temporal offset separately for each device and recording session. Specifically, we search over offsets within a 10-second window relative to the Polar H10 and select the offset that minimizes MAE. We apply the same procedure to SwimHR and all wearable baselines to ensure a consistent and conservative comparison.

Overall Accuracy and Stability. Across all valid recordings, SwimHR achieves the lowest HR estimation error, while also providing the most consistent performance across recordings. As shown in Figure 8, SwimHR attains an MAE of 1.0 bpm with a standard deviation of 0.9 bpm, both significantly lower than those of the wearable baselines. In contrast, the wearable baselines exhibit both higher errors and substantially higher performance variability. The Apple Watch, Polar Verity Sense (forearm and temple) achieve MAEs of 5.4 bpm, 3.0 bpm, and 4.4 bpm, respectively, with corresponding standard deviations of 7.7 bpm, 5.2 bpm, and 8.8 bpm. The Apple Watch produces sparse HR updates during swimming,

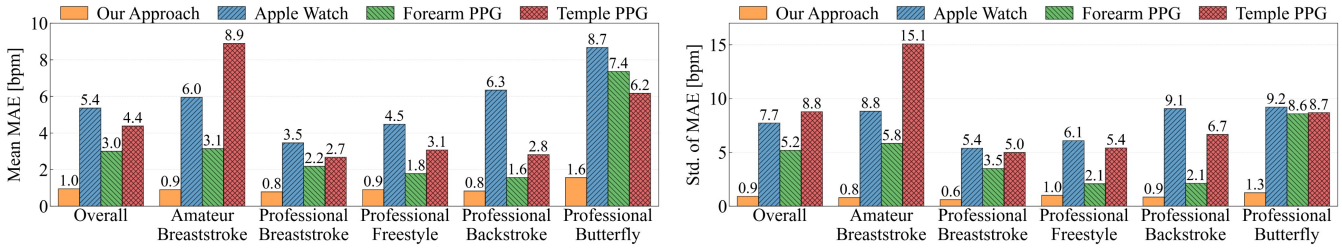

(a) Mean MAE by category **(b) Standard deviation of MAE by category**

Figure 8: Heart rate estimation performance across swimmer groups and swimming strokes.

sometimes maintaining the same value for extended periods, which leads to higher MAE and large temporal fluctuations after forward filling. The Polar Verity Sense provides denser HR estimates but remains sensitive to motion artifacts and sensor placement variability.

Importantly, unlike the evaluated wearables, including the ground-truth ECG chest band, which store data locally and provide HR only after the swimming session, SwimHR places its acquisition and wireless communication units on the pool deck, enabling continuous real-time HR output. Combined with its accurate estimates, SwimHR can support in-session feedback for coaches without requiring any on-body device.

Performance Across Swimming Strokes. We next evaluate performance across four competitive strokes using data from 22 professional swimmers. SwimHR achieves the lowest MAE across all stroke settings: 0.8 bpm for breaststroke, 0.9 bpm for freestyle, 0.8 bpm for backstroke, and 1.6 bpm for butterfly (Figure 8(a)). In addition to lower mean error, SwimHR also exhibits substantially lower MAE variability, indicating better performance consistency across recordings.

Among the four strokes, butterfly is the most challenging for all systems because its large upper-body movements and dolphin kicks generate substantial motion artifacts and water turbulence. These conditions significantly degrade the performance of wearable PPG sensors, which are highly sensitive to motion-induced changes in the optical path. As shown in Figure 8, the MAEs of the temple-mounted PPG sensor and Apple Watch increase to 6.2 bpm and 8.7 bpm, respectively, with corresponding error standard deviations of 8.7 bpm and 9.2 bpm. In contrast, SwimHR maintains an MAE of 1.6 bpm and a standard deviation of 1.3 bpm. This robustness stems from stationary pool-mounted sensing and robust HR extraction, enabling it to better tolerate stroke-dependent motion artifacts.

To further illustrate the robustness of SwimHR, Figure 9 shows representative heart-rate traces for one professional swimmer across all four competitive strokes. The HR estimated by SwimHR closely follows the Polar H10 ground-truth reference across all strokes. In contrast, the wearable PPG baselines exhibit larger deviations and unstable behavior. In particular, during freestyle, the temple- and forearm-mounted PPG show substantial drift and the Apple Watch produces sparse updates, while SwimHR maintains consistent tracking of HR changes. These examples are consistent with the quantitative results in Figure 8, demonstrating that SwimHR provides both accurate and temporally stable HR estimates during active swimming across all four strokes.

Performance Across Swimmer Groups. We further compare the performance of SwimHR across swimmer populations with different skill levels. For amateur swimmers, who perform breaststroke only, SwimHR achieves an MAE of 0.9 bpm across 12 participants compared with 0.8 bpm for the 22 professional swimmers in breaststroke. These comparable results indicate consistent performance across swimmer groups despite differences in swimming proficiency.

In contrast, the wearable baselines exhibit a noticeably larger performance gap between amateur and professional swimmers (Figure 8). For example, the temple-mounted PPG sensor shows an MAE of 8.9 bpm for amateur breaststroke but improves to 2.7 bpm for professional swimmers. A likely reason is that professional swimmers are more experienced with such devices and can maintain more stable goggle fit and sensor contact. This effect is particularly evident for temple-mounted PPG sensing, whose performance depends strongly on the goggle fit and sensor contact, both of which may vary substantially across users.

This comparison highlights an important advantage of SwimHR over wearable approaches: it does not require swimmers to wear or adjust any device. Users can simply enter the pool and swim, while SwimHR continuously measures HR without relying on prior experience with wearable sensors.

5.3 System Micro-benchmarks

Peak Detection Performance. We evaluate the contribution of the U-Net detector by replacing only Stage 2 of Algorithm 1 with a conventional NeuroKit2 baseline, while keeping adaptive channel selection and temporal consistency filtering unchanged. For each selected channel, we apply `ecg_peaks()` to both the original and polarity-inverted

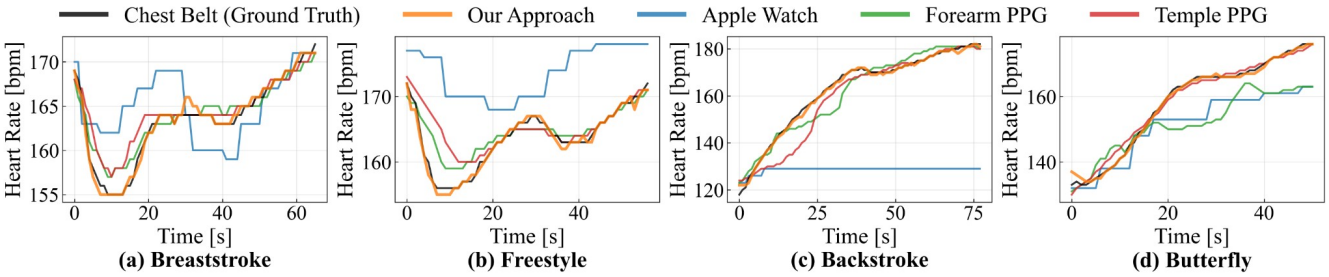

Figure 9: Representative heart rate traces for one professional swimmer across all four strokes.

Table 2: Mean ± std of HR MAE (bpm) using the NeuroKit2 and U-Net R-peak detection.

	NeuroKit2	U-Net
Overall	1.30 ± 1.66	**0.95 ± 0.92**
Amateur breaststroke	1.18 ± 1.12	**0.90 ± 0.79**
Professional breaststroke	0.96 ± 0.93	**0.78 ± 0.61**
Professional freestyle	1.00 ± **0.90**	**0.90** ± 1.01
Professional backstroke	1.27 ± 2.29	**0.83 ± 0.85**
Professional butterfly	2.46 ± 2.47	**1.56 ± 1.25**

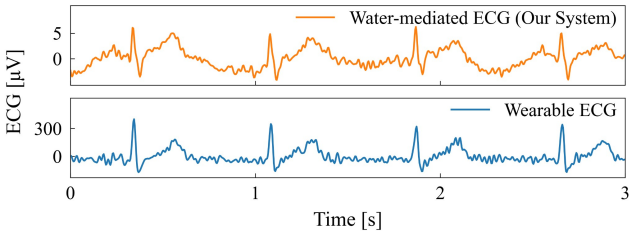

Figure 10: Simultaneously recorded water-mediated and reference ECG signals, filtered at 1–50 Hz.

signals, and merge detections within 0.1 s by retaining the largest absolute amplitude peak.

We evaluate both detectors using leave-one-swimmer-out cross-validation on 170 manually annotated recordings, five 50 m breaststroke trials per swimmer, totaling 8,500 m. Following prior evaluations [24, 28], a detection is correct if it falls within ±50 ms of an unmatched reference R-peak. Without temporal filtering, the U-Net achieves an F_1 score of 0.96, compared with 0.92 for NeuroKit2; with filtering, the scores improve to 0.97 and 0.93, respectively. These results show that the U-Net provides more accurate R-peak detection than the conventional baseline, while temporal consistency filtering further reduces residual detection errors.

We further compare their HR estimation performance across swimmer groups and strokes. As shown in Table 2, the U-Net yields lower mean MAE in every category and lower variability in most cases. The improvement is most pronounced for butterfly, where MAE decreases from 2.46 ± 2.47 bpm to 1.56 ± 1.25 bpm, and for backstroke, where it decreases from 1.27 ± 2.29 bpm to 0.83 ± 0.85 bpm. These results show that the U-Net improves both R-peak localization and stroke-robust HR estimation, with particular benefits under high-motion conditions such as butterfly.

ECG Validity. To validate our water-mediated ECG sensing, we conduct a controlled experiment with one swimmer. The participant floats on the water surface while holding the pool edge, maintaining a stable swimming posture with the body parallel to the pool bottom. We simultaneously record two ECG signals for three minutes: (1) water-mediated ECG acquired by SwimHR, and (2) a reference ground truth ECG collected using gel electrodes attached to both arms above the water surface. Under this controlled experiment, we apply a 1–50 Hz bandpass filter to both recordings to preserve the P-wave, QRS-complex, and T-wave morphology. In contrast, the R-peak detection pipeline uses a 10–30 Hz filter during active swimming to suppress motion artifacts and emphasize the QRS complex.

We evaluate temporal alignment by detecting R-peaks in both signals and computing the sample-wise timing error between corresponding peaks. The mean R-peak timing error is 0.65 samples, equivalent to 5.2 ms at a 125 Hz sampling rate, demonstrating that water-mediated ECG sensing preserves the temporal fidelity required for accurate HR estimation. Figure 10 shows an example of two simultaneously recorded ECG signals, where R-peaks align closely despite slight waveform differences caused by different lead configurations.

Different Swimming Pool Comparison. To evaluate cross-pool generalization, three skilled amateur swimmers (S1–S3) each complete a 500 m breaststroke session in both Pool A and Pool B. As shown in Table 3, the MAE remains low and comparable, averaging 1.02 bpm in Pool A and 0.68 bpm in Pool B. This result is notable because the pools differ in both depth profile and water conductivity, two factors that directly affect ECG transmission as discussed in Section 3.1. Overall, these results indicate that SwimHR maintains reliable HR estimation across swimming pool environments.

Table 3: MAE [bpm] of three swimmers across pools.

	S1	S2	S3	Mean
Pool A	1.33	0.88	0.85	1.02
Pool B	0.92	0.56	0.55	0.68

5.4 System Usability

Evaluated Sensing Range. In our study setup, the target swimmer remained within ±1.25 m of the sensing electrodes, corresponding to half the width of the 2.5m-wide lane. Adjacent lanes remained open for normal pool use, and some sessions included swimmers in neighboring lanes. We observed no noticeable difference in the captured ECG signals or HR estimation accuracy between sessions with and without adjacent-lane swimmers, indicating negligible interference under the evaluated deployment geometry.

Power Usage. The system operates at a measured current of approximately 40 mA during continuous sensing and wireless transmission. With a tiny 500 mAh LiPo battery, this corresponds to about 12.5 hours of continuous operation, which is sufficient to support multiple swimming sessions within a single deployment.

User Interview. In addition to quantitative evaluation, we collected user feedback on both the SwimHR system and the wearable baselines through a post-study questionnaire. Participants rated their experience using a 5-point Likert scale (1: Strongly Disagree, 5: Strongly Agree) based on the following statements:

- Q1: I found the system/wearables comfortable to use.
- Q2: I like the experience of using the system/wearable.
- Q3: I prefer the SwimHR system to the wearable devices.

Overall, participants reported higher satisfaction with the SwimHR system than with wearable devices (Figure 11(a)). The most commonly cited reasons were improved comfort and the absence of body-worn sensors that could interfere with swimming movements. Figure 11(b) shows the skin marks left by tightly worn wearables, illustrating the discomfort associated with such devices. Professional swimmers in particular noted that wearable devices often shift or detach during high-intensity strokes, which can both affect swimming performance and reduce measurement reliability.

We also asked participants whether they would be willing to use our system during regular training. Most participants indicated that they would continue using it because it allows them to swim without wearing any sensors. Only three participants expressed hesitation, primarily due to concerns about accidental contact with the system. To quantify this risk, we recorded all contact events during the experiments and observed only one instance of accidental contact across all sessions, which did not cause any injury or discomfort.

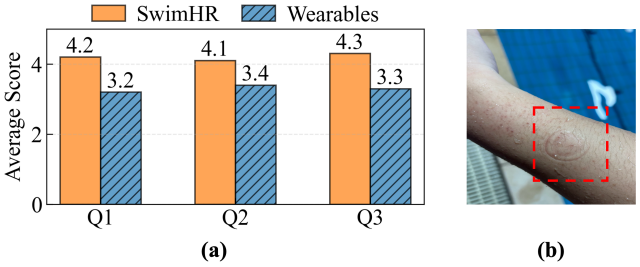

Figure 11: (a) User ratings comparison between SwimHR and wearable devices. (b) Skin indentation from a tightly worn Polar Verity Sense.

We discuss possible design improvements to further reduce such concerns in Section 6.

6 Discussions and Future Work

Limitations. We evaluate SwimHR only in pools up to 1.6 m deep, using a research prototype that holds the electrodes 1 m below the water surface. Our results therefore do not establish performance or deployment practicality in deeper competition pools, where alternative mounting structures may be required. Future work will explore lower-profile, adjustable-depth, and lane-divider-integrated designs. Although most participants were willing to use the system, some expressed concerns about accidental contact with the underwater hardware. Future designs could reduce the physical profile of the electrode support or integrate the prototype into existing pool infrastructure to minimize exposed components and improve user confidence in the system.

Localizing the Swimmer. Beyond heart-rate monitoring, the transmission model derived in Section 3.1 suggests that the amplitude of the received ECG signal varies systematically with the swimmer–electrode distance. As a swimmer moves along the lane, the ECG signal strength observed at different electrode pairs changes according to this geometric relationship. In principle, this spatial variation could be leveraged to estimate the swimmer's position by identifying the electrode pairs that observe the strongest signals or by fitting the observed amplitudes to the model. The localization granularity depends on the quality of the captured ECG signals and the density of deployed electrodes. While we do not explore this capability in this work, it opens the possibility of extending SwimHR to support swimmer localization and lane-level activity analytics in future systems.

Multiple Swimmers within Sensing Range. Another noteworthy capability of the proposed sensing principle is capturing ECG signals from multiple swimmers simultaneously. Figure 12 illustrates an example where two stationary swimmers are present in the same lane. The signal captured by the lane-rope channel shows a mixture of ECG waveforms from both swimmers, while the reference channels confirm

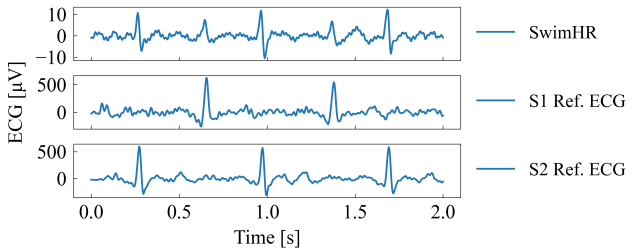

Figure 12: Example of mixed ECG signals when two swimmers are present in the same lane. SwimHR captures a superposition of both swimmers' ECG signals.

the individual ECG signals. This result demonstrates that the sensing mechanism can capture multiple cardiac sources within the same sensing region. In principle, the mixed signal could potentially be separated to recover individual ECG traces using source-separation techniques combined with the spatial structure of our electrode deployment. Our presented user study considers only one swimmer per instrumented lane. Recovering individual HRs from moving swimmers would require source separation and identity association, which we leave to future work.

7 Related Work

Underwater ECG Sensing. Prior work has explored underwater ECG sensing using two main approaches: contact-based sensing [6, 45, 50, 58] and non-contact sensing [19, 25, 26, 39, 47, 62, 63]. Contact-based methods rely on electrodes directly attached to the skin [6, 50]. Prior work has focused on developing specialized electrodes [45, 58] to mitigate the limitations of traditional gel electrodes, which tend to lose adhesion in water. However, these approaches still require swimmers to wear sensing devices, which may interfere with performance. Non-contact approaches instead exploit the conductivity of water to transmit ECG signals to electrodes positioned away from the body [19, 25, 39, 47]. This phenomenon has been demonstrated primarily in confined environments such as bathtubs. For example, Xu et al. [62, 63] used non-contact ECG signals for identity recognition to improve bathing safety, while Li et al. [26] extracted heart-rate variability from bathtub ECG signals to assess stress levels. In contrast, we extend this non-contact sensing principle to large aquatic environments. To the best of our knowledge, our work is the first to establish and validate a theoretical model of ECG transmission through water and demonstrate ECG sensing in real swimming conditions.

Underwater HR Monitoring. Accurate heart-rate monitoring is important for both swimmer safety and performance optimization in aquatic sports. Existing underwater HR monitoring systems mainly rely on PPG-based sensing or ECG-based sensing. PPG sensors estimate heart rate by emitting light onto the skin and measuring variations in reflected or transmitted light intensity [56]. Commercial smartwatches, such as the Apple Watch [1], provide wrist-based optical HR monitoring during swimming, while swimming-oriented optical sensors such as the Polar Verity Sense can be worn on the arm or mounted on a swimming-goggle strap near the temple [44]. Prior evaluations have shown that the performance of optical wearables depends strongly on sensor placement, fit, and swimming intensity [2, 4, 7, 40].

ECG-based HR monitoring estimates heart rate by detecting R-peaks in the ECG waveform [42]. Commercial chest straps, such as the Polar H10 [43], and research prototypes [6, 20, 45] both rely on on-body electrodes to measure ECG signals and compute HR from the intervals between detected R-peaks. Other approaches use alternative sensing modalities, such as acceleration and pressure sensors [27]. However, these methods impose a wearable burden and constrain swimmers' movements, making them inconvenient in aquatic environments. In contrast, SwimHR uses pool-mounted electrodes and a pool-deck acquisition unit to estimate HR without placing any device on the swimmer.

8 Conclusion

We present SwimHR, the first wearable-free system for continuously monitoring swimmers' heart rate in standard swimming pools via water-mediated ECG. SwimHR combines a pool-scale transmission model, a deployable lane-scale sensing hardware design, and a spatial-temporal HR extraction pipeline to enable accurate and stable HR estimation without requiring any on-body device. We evaluate SwimHR with 34 swimmers across two public pools and four competitive strokes, and show that it achieves accurate HR monitoring while substantially outperforming commercial wearables. These results demonstrate the promise of aquatic infrastructure as a practical substrate for wearable-free physiological sensing and open new opportunities for training analytics and unobtrusive health monitoring in water.

Acknowledgments

We thank the anonymous reviewers for their constructive feedback and all participants for their contributions. We also thank the Sports Science and Technology Research Centre at HKUST and Diocesan Girls' School for providing swimming-pool access and support. This work was supported in part by the Hong Kong Center for Construction Robotics (InnoHK-HKCRC), an InnoHK center funded by the Hong Kong Innovation and Technology Commission. The views expressed are those of the authors and do not necessarily reflect those of the funding agencies or supporting organizations.

References

[1] Apple Inc. 2021. Apple Watch Series 7 – Technical Specifications. (2021). Retrieved Jul 26, 2026 from https://support.apple.com/en-us/111909

[2] Behnam Askarian, Kwanghee Jung, and Jo Woon Chong. 2019. Monitoring of heart rate from photoplethysmographic signals using a Samsung Galaxy Note8 in underwater environments. *Sensors* 19, 13 (2019), 2846.

[3] Branko Babusiak, Stefan Borik, and Maros Smondrk. 2020. Two-electrode ECG for ambulatory monitoring with minimal hardware complexity. *Sensors* 20, 8 (2020), 2386.

[4] Raul F Bartolomeu, Vasco Silva, Ana Pereira, Gonçalo Morais, Kamil Sokołowski, Marek Strzała, Jorge E Morais, and José E Teixeira. 2025. Agreement between a wristwatch and a free optical sensor with a chest strap in measuring HR variations during front crawl swimming. *Applied Sciences* 15, 11 (2025), 5848.

[5] M Burrows. 1974. Motion-induced noise in electrode-pair extremely low frequency (ELF) receiving antennas. *IEEE Transactions on Communications* 22, 4 (1974), 540–542.

[6] Tobias Cibis, Benjamin H Groh, Heike Gatermann, Heike Leutheuser, and Bjoern M Eskofier. 2015. Wearable real-time ecg monitoring with emergency alert system for scuba diving. In *2015 37th Annual International Conference of the IEEE Engineering in Medicine and Biology Society (EMBC)*. IEEE, 6074–6077.

[7] Gloria Cosoli, Luca Antognoli, Valentina Veroli, and Lorenzo Scalise. 2022. Accuracy and precision of wearable devices for real-time monitoring of swimming athletes. *Sensors* 22, 13 (2022), 4726.

[8] Ipswich City Council. 2025. Equipotential Bonding Around a Swimming Pool. (2025). Retrieved Jul 17, 2025 from https://www.ipswich.qld.gov.au/__data/assets/pdf_file/0010/259840/EquipotentialBonding_FactSheet_2.pdf

[9] Axel Tcheheumeni Djanni, Anton Ziolkowski, and David Wright. 2016. Electromagnetic induction noise in a towed electromagnetic streamer. *Geophysics* 81, 3 (2016), E187–E199.

[10] Anthony Dupre, Sarah Vincent, and Paul A Iaizzo. 2005. Basic ECG theory, recordings, and interpretation. Springer, 191–201.

[11] Hilko Ehmen, Marten Haesner, Ines Steinke, Mario Dorn, Mehmet Gövercin, and Elisabeth Steinhagen-Thiessen. 2012. Comparison of four different mobile devices for measuring heart rate and ECG with respect to aspects of usability and acceptance by older people. *Applied ergonomics* 43, 3 (2012), 582–587.

[12] Jonathan Friedman, Dustin Torres, Thomas Schmid, Juyao Dong, and Mani B Srivastava. 2010. A biomimetic quasi-static electric field physical channel for underwater ocean networks. In *Proceedings of the 5th International Workshop on Underwater Networks*. 1–8.

[13] David J Griffiths. 2023. *Introduction to electrodynamics*. Cambridge University Press.

[14] Marco Guermandi, Eleonora Franchi Scarselli, and Roberto Guerrieri. 2015. A driving right leg circuit (DgRL) for improved common mode rejection in bio-potential acquisition systems. *IEEE transactions on biomedical circuits and systems* 10, 2 (2015), 507–517.

[15] David Halliday, Robert Resnick, and Jearl Walker. 2008. *Fundamentals of physics*. Wiley New York.

[16] John Hampton, Joanna Hampton, and David Adlam. 2024. *The ECG Made Easy*. Elsevier Health Sciences.

[17] Mike Holt. 2015. Article 680—Swimming Pools, Spas, Hot Tubs, Fountains, and Similar Installations. (2015). Retrieved Jul 17, 2025 from https://windsorlocksct.org/wp-content/uploads/2020/09/Swimming_Pools_and_Spas_2014NEC.pdf

[18] Texas Instruments. 2017. ADS1299-x Low-Noise, 4-, 6-, 8-Channel, 24-Bit, Analog-to-Digital Converter for EEG and Biopotential Measurements. (2017). Retrieved Jul 28, 2025 from https://www.ti.com.cn/cn/lit/gpn/ads1299

[19] M Ishijima and T Togawa. 1989. Observation of electrocardiograms through tap water. *Clinical Physics and Physiological Measurement* 10, 2 (1989), 171.

[20] Robert Shukri Habib Istepanian and Bryan Woodward. 1997. Microcontroller-based underwater acoustic ECG telemetry system. *IEEE transactions on information technology in biomedicine* 1, 2 (1997), 150–154.

[21] Atte Joutsen, Alper Cömert, Emma Kaappa, Kirsi Vanhatalo, Jarno Riistama, Antti Vehkaoja, and Hannu Eskola. 2024. ECG signal quality in intermittent long-term dry electrode recordings with controlled motion artifacts. *Scientific Reports* 14, 1 (2024), 8882.

[22] Atte S Joutsen, Emma S Kaappa, Tapio J Karinsalo, and Jukka Vanhala. 2018. Dry electrode sizes in recording ECG and heart rate in wearable applications. In *EMBEC & NBC 2017*. IFMBE Proceedings, Vol. 65. Springer, 735–738. https://doi.org/10.1007/978-981-10-5122-7_184

[23] KEDIDA. 2016. Conductivity meter CT-3030. (2016). Retrieved Jul 25, 2025 from http://www.kedida.com.cn/en/category/conductivitymeterseries/101.html

[24] Vessela Krasteva, Ivo Iliev, and Serafim Tabakov. 2024. Application of convolutional neural network for decoding of 12-lead electrocardiogram from a frequency-modulated audio stream (sonified ECG). *Sensors* 24, 6 (2024), 1883.

[25] Subhash C Kwatra and Vijay K Jain. 1986. A new technique for monitoring heart signals-part I: instrumentation design. *IEEE transactions on biomedical engineering* 1 (1986), 35–41.

[26] Tianhui Li and Wenxi Chen. 2022. Bathtub ECG as a Potential Alternative to Light Stress Test in Daily Life. *Electronics* 11, 9 (2022), 1310.

[27] Hibisca Liaw. 2013. *Underwater Measurements of Heart Rate*. Ph.D. Dissertation. Georgia Institute of Technology.

[28] Feifei Liu, Chengyu Liu, Xinge Jiang, Zhimin Zhang, Yatao Zhang, Jianqing Li, and Shoushui Wei. 2018. Performance analysis of ten common QRS detectors on different ECG application cases. *Journal of healthcare engineering* 2018, 1 (2018), 9050812.

[29] Dominique Makowski, Tam Pham, Zen J. Lau, Jan C. Brammer, François Lespinasse, Hung Pham, Christopher Schölzel, and S. H. Annabel Chen. 2021. NeuroKit2: A Python toolbox for neurophysiological signal processing. *Behavior Research Methods* 53, 4 (feb 2021), 1689–1696. https://doi.org/10.3758/s13428-020-01516-y

[30] Cyrus G Malmberg and Arthur A Maryott. 1956. Dielectric constant of water from 0 to 100 C. *Journal of research of the National Bureau of Standards* 56, 1 (1956), 1–8.

[31] M Sabarimalai Manikandan and KP Soman. 2012. A novel method for detecting R-peaks in electrocardiogram (ECG) signal. *Biomedical signal processing and control* 7, 2 (2012), 118–128.

[32] Pratheek Michael. 2017. *Simulation Studies on ECG Vector Dipole Extraction in Liquid Medium*. Master's thesis. University of South Florida.

[33] David M Mirvis and Ary L Goldberger. 2001. Electrocardiography. Vol. 1. WB Saunders, Philadelphia, 82–128.

[34] COMSOL Multiphysics. 2025. Simulate real-world designs, devices, and processes with multiphysics software from COMSOL. (2025). Retrieved Jul 23, 2025 from https://www.comsol.com/

[35] Umar Farouk Mustapha, Seth Mensah Abobi, and Gerard Quarcoo. 2020. Physicochemical and bacteriological quality of public swimming pools in the Tamale Metropolis, Ghana. *J* 3, 2 (2020), 18.

[36] Freddy Odille, Shufang Liu, Peter van Dam, and Jacques Felblinger. 2017. Statistical variations of heart orientation in healthy adults. In *2017 Computing in Cardiology (CinC)*. IEEE, 1–4.

[37] The Government of the Hong Kong Special Administrative Region. 2017. General Specification for Swimming Pool Water Treatment Installation in Government Buildings of the Hong Kong Special Administrative Region. (2017). Retrieved Jul 20, 2025 from https://www.archsd.gov.hk/media/publications-publicity/general-specification-for-swimming-pool-water-treatment-installation/spgs2017.pdf

[38] The Government of Western Australia. 2025. Swimming pools and spas: electrical bonding. (2025). Retrieved Jul 17, 2025 from https://www.wa.gov.au/government/multi-step-guides/electrical-safety-home/swimming-pools-and-spas-electrical-bonding

[39] Mitsuhiro Ogawa, Yuichi Kimura, Toshiyo Tamura, and Tatsuo Togawa. 1996. Fully automated ECG data acquisition in a bathtub. In *Proceedings of 18th Annual International Conference of the IEEE Engineering in Medicine and Biology Society*, Vol. 1. IEEE, 55–56.

[40] Bjørn Harald Olstad and Christoph Zinner. 2020. Validation of the Polar OH1 and M600 optical heart rate sensors during front crawl swim training. *PLoS One* 15, 4 (2020), e0231522.

[41] OpenBCI. 2025. Cyton Biosensing Board (8-Channels). (2025). Retrieved Jul 25, 2025 from https://shop.openbci.com/products/cyton-biosensing-board-8-channel

[42] Jakub Parák and Jan Havlík. 2011. ECG signal processing and heart rate frequency detection methods. *Proceedings of Technical Computing Prague* 8 (2011), 2011.

[43] Polar. [n. d.]. Does H10 Measure Heart Rate When Swimming? ([n. d.]). Retrieved Jul 26, 2026 from https://support.polar.com/en/support/does_h10_measure_heart_rate_when_swimming

[44] Polar. [n. d.]. Polar Verity Sense User Manual: Wearing Your Verity Sense. ([n. d.]). Retrieved Jul 26, 2026 from https://support.polar.com/e_manuals/verity-sense/polar-verity-sense-user-manual-english/wearing-your-verity-sense.htm

[45] Bersain A Reyes, Hugo F Posada-Quintero, Justin R Bales, Amanda L Clement, George D Pins, Albert Swiston, Jarno Riistama, John P Florian, Barbara Shykoff, Michael Qin, et al. 2014. Novel electrodes for underwater ECG monitoring. *IEEE Transactions on Biomedical Engineering* 61, 6 (2014), 1863–1876.

[46] Saaz Kaur Sahdra, Grant Duthie, Judy Kay, and Kalina Yacef. 2024. Monitoring Physical Health, Mental Health, Nutrition, and Sleep in Athletes to Improve Performance: Workshop Position Paper: Multimodal Sports Interaction: Wearables and HCI in Motion. In *Companion of the 2024 on ACM International Joint Conference on Pervasive and Ubiquitous Computing*. 444–449.

[47] Tsunemasa Saiki, Yukako Takizawa, Koji Murai, Ryuhei Okuno, and Masakazu Arima. 2021. A novel method for noninvasive bioelectric measurement utilizing conductivity of seawater. *Scientific reports* 11, 1 (2021), 7073.

[48] Franciska M Schets, Harold HJL van Den Berg, Gretta Lynch, Sharona de Rijk, Ana Maria de Roda Husman, and Jack F Schijven. 2020. Evaluation of water quality guidelines for public swimming ponds. *Environment international* 137 (2020), 105516.

[49] Laurent Schmitt, Jacques Regnard, Denis Auguin, and Gregoire P Millet. 2016. Monitoring training and fatigue with heart rate variability: case study in a swimming Olympic champion. *Journal of fitness research* 5, 3 (2016), 38–45.

[50] Andreas Schuster, Olivier Castagna, Bruno Schmid, Tobias Cibis, Arne Sieber, et al. 2017. Underwater monitoring system for body temperature and ECG recordings. *Underwater Technology* 34, 3 (2017), 135–139.

[51] Qijia Shao. 2024. Weaving Physical and Physiological Sensing with Computational Fabrics. In *Proceedings of the 22nd Annual International Conference on Mobile Systems, Applications and Services (MOBISYS '24)*. Association for Computing Machinery, New York, NY, USA, 748–750. https://doi.org/10.1145/3643832.3661385

[52] Qijia Shao, Junxiao Chen, Ho Man Colman Leung, Meiqi Zhao, Ruoyu Xu, Jiting Liu, Lisa Maria DiSalvo García, Xiaofan Jiang, Marie-Pierre St-Onge, and Xia Zhou. 2025. My Pillow Knows My Sleep: Sleep Monitoring with Computational Fabrics in the Pillowcase. *Proc. ACM Interact. Mob. Wearable Ubiquitous Technol.* 9, 3, Article 128 (Sept. 2025), 26 pages. https://doi.org/10.1145/3749550

[53] Qijia Shao, Jiting Liu, Emily Bejerano, Ho Man Colman, Jingping Nie, Xiaofan Jiang, and Xia Zhou. 2024. Joey: Supporting Kangaroo Mother Care with Computational Fabrics. In *Proceedings of the 22nd Annual International Conference on Mobile Systems, Applications and Services (MOBISYS '24)*. Association for Computing Machinery, New York, NY, USA, 237–251. https://doi.org/10.1145/3643832.3661867

[54] Penghang Shuai, Haipeng Li, Chao Zhou, Yaming Ou, Zhuoliang Zhang, Chunhui Zhu, and Junfeng Fan. 2025. Mapping and Localization in Unknown Underwater Electric Field Using Passive Electric Sense System. *IEEE Transactions on Instrumentation and Measurement* 74 (2025), 1–12. https://doi.org/10.1109/TIM.2025.3548185

[55] Siniša Sovilj, Ratko Magjarević, Nigel H Lovell, and Socrates Dokos. 2013. A simplified 3D model of whole heart electrical activity and 12-lead ECG generation. *Computational and mathematical methods in medicine* 2013, 1 (2013), 134208.

[56] Andriy Temko. 2017. Accurate heart rate monitoring during physical exercises using PPG. *IEEE Transactions on Biomedical Engineering* 64, 9 (2017), 2016–2024.

[57] Larisa G Tereshchenko and Mark E Josephson. 2015. Frequency content and characteristics of ventricular conduction. *Journal of electrocardiology* 48, 6 (2015), 933–937.

[58] Tharoeun Thap, Kwon-Ha Yoon, and Jinseok Lee. 2016. Graphite based electrode for ECG monitoring: Evaluation under freshwater and saltwater conditions. *Sensors* 16, 4 (2016), 542.

[59] Anthony J Weinhaus and Kenneth P Roberts. 2009. Anatomy of the human heart. In *Handbook of cardiac anatomy, physiology, and devices*. Springer, 59–85.

[60] Bruce B Winter and John G Webster. 1983. Driven-right-leg circuit design. *IEEE Transactions on biomedical engineering* 1 (1983), 62–66.

[61] Xu Xie, Hao Zuo, Shize Wei, and Qin Wu. 2023. Motion-induced noise detection of electrode-pair towed antennas using helix coil sensors. *Electronics* 12, 7 (2023), 1677.

[62] Jianbo Xu and Wenxi Chen. 2022. Convolutional Neural Network-Based Identity Recognition Using ECG at Different Water Temperatures During Bathing. *Computers, Materials & Continua* 71, 1 (2022). https://doi.org/10.32604/cmc.2022.021154

[63] Jianbo Xu, Peng Cui, and Wenxi Chen. 2020. ECG-based identity validation during bathing in different water temperature. In *2020 42nd Annual International Conference of the IEEE Engineering in Medicine & Biology Society (EMBC)*. IEEE, 5276–5279.

[64] Muhammad Uzair Zahid, Serkan Kiranyaz, Turker Ince, Ozer Can Devecioglu, Muhammad EH Chowdhury, Amith Khandakar, Anas Tahir, and Moncef Gabbouj. 2021. Robust R-peak detection in low-quality holter ECGs using 1D convolutional neural network. *IEEE Transactions on Biomedical Engineering* 69, 1 (2021), 119–128.

[65] Yuzhong Zhang, Zhenyi Zhao, Xinglong Feng, Tianyi Zhao, and Qiao Hu. 2024. Implementation of underwater electric field communication based on direct sequence spread spectrum (dsss) and binary phase shift keying (bpsk) modulation. *Biomimetics* 9, 2 (2024), 103.

[66] Donald W Zipse. 2006. Equipotential Planes, a Figment of the Imagination. In *2006 IEEE Industrial and Commercial Power Systems Technical Conference-Conference Record*. IEEE, 1–17.

A ECG Simulation

Our simulation model consists of two components: a 3-D model of cardiac electrical activity [55] and a swimming pool environment. The cardiac electrical model, obtained via email from the authors, includes the torso, lungs, and the entire heart, including atria, ventricles, and blood chambers, as shown in Fig. 13. The heart structures, such as atria and ventricles, serve as the electrical source and form the basis for ECG signal generation, while other structures, including the blood chamber, lung and torso, are passive volume conductors. The FitzHugh-Nagumo equations are modified to define cellular activation of the heart structures. More details about the equations and the geometric dimensions can be found in the original paper.

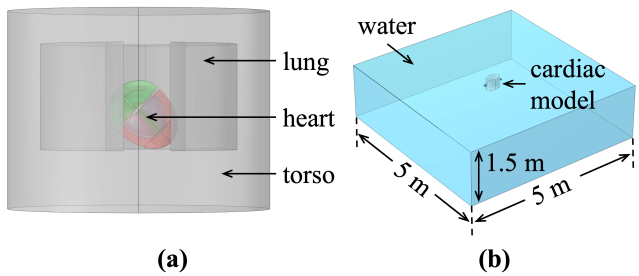

Figure 13: (a) The 3-D cardiac electrical activity model. (b) The cardiac model is immersed in a pool to simulate ECG transmission through water.

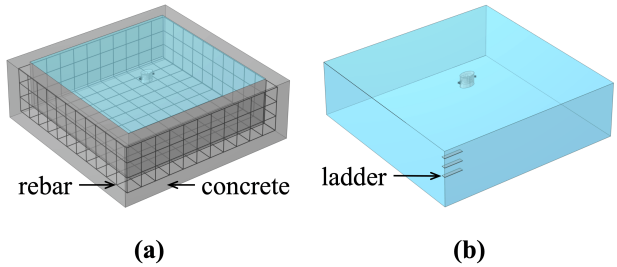

Figure 14: (a) The reinforcing steel and concrete walls surrounding the swimming pool. (b) The stainless-steel ladder is at the corner of the pool.

The swimming pool environment, designed by us, is used as a passive conductor to simulate the transmission of ECG signals through water. The pool measures $5m \times 5m \times 1.5m$ and is filled with water that has a conductivity of $0.05 S/m$. The cardiac model is immersed to a depth of 0.2 m at the center of the pool, and the voltage difference between two points is measured to obtain the ECG waveforms. Two points are positioned 0.5m apart on the left and right sides of the body, with the body located at the midpoint and the electrodes placed at half the height of the torso. According to the discussion on the pool's environmental influences in section 3.1, the corresponding parameters are modified to quantify their influences:

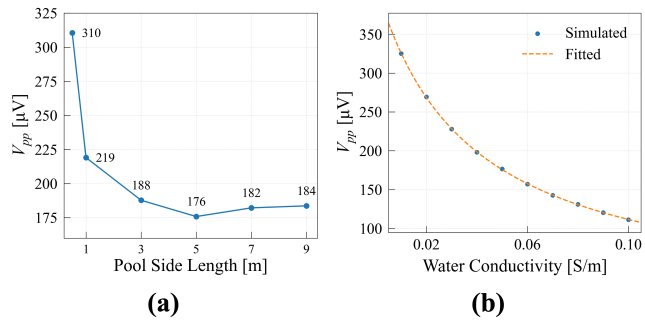

Figure 15: (a) The relationship between signal strength and various pool sizes. (b) The relationship between signal strength and different water conductivities.

(1) Water Volume: The dimensions of the swimming pool vary from $0.5m \times 0.5m$, $1m \times 1m$, $3m \times 3m$, $5m \times 5m$, to $9m \times 9m$ while maintaining a constant depth. The cardiac model remains centered in the pool regardless of its dimensions. As shown in Figure 15(a), signal strength decreases with pool dimensions, but the attenuation rate plateaus once dimensions exceed $3\,m \times 3\,m$.

(2) Water Conductivity: The pool water's conductivity is increased from 0.01 to 0.1 S/m in increments of 0.01 S/m, while the pool's dimensions are fixed at $5m \times 5m \times 1.5m$. As illustrated in Figure 15(b), when the dimensions of the swimming pool are fixed, higher conductivity results in greater attenuation of signal strength.

(3) Pool Safety Measures: To simulate the reinforcing steel and concrete walls, the swimming pool is surrounded by concrete walls with a thickness of 0.5 m, which contain reinforcing bars set to 0 V. The spacing between the reinforcing bars is 0.5 m, and the radius of the bars is 8 mm. As shown in Fig. 14(a), the grey area represents the concrete wall, while the grid within it is the reinforcing steel. To simulate the pool ladders, three stainless-steel steps are positioned at the corner of the pool, as shown in Fig. 14(b). Each step is 50 cm in length, 10 cm in width, and 1 cm in thickness, with a distance of 25 cm between adjacent steps. The steps are set to 0 V. The reinforcing bars reduce V_{pp} from 176 μV to 172 μV, causing negligible signal attenuation. In contrast, pool ladders significantly decrease V_{pp} to 66 μV, reducing signal strength to 38% of the original value.